


Article

Vibration Characteristic Research of 100 m New Polar Exploration Cruise Based on Finite Element Modeling

Guohe Jiang, Yuhao Yuan, Hao Guo *, Gang Wu  and Zhenzhen Liu

Merchant Marine College, Shanghai Maritime University, Shanghai 201306, China;
guohejiang@shmtu.edu.cn (G.J.); 202230110126@stu.shmtu.edu.cn (Y.Y.); wugang@shmtu.edu.cn (G.W.);
202230210313@stu.shmtu.edu.cn (Z.L.)

* Correspondence: guohao@shmtu.edu.cn

Abstract: Luxury cruise ships are high-end passenger ships with facilities on board for the leisure and entertainment of passengers, so the comfort of luxury cruise ships is a matter of great concern. In this paper, a finite element model of a new polar exploration cruise ship is established, and the wet modes of the whole ship are calculated using the virtual mass method and compared with the principal frequencies of the excitation forces to initially verify the rationality of the design of the structural vibration characteristics of the whole ship. The admittance matrix of the vibration velocity to excitation force was calculated by a frequency response analysis, and the vibration velocities at the stern plate and main engine foundations were tested during sailing. Then, the obtained propeller and main engine excitation forces were loaded into the finite element model; the vibration velocities of each compartment were calculated and compared with the compartment vibration velocity test values. The errors were within the engineering allowable range, verifying the accuracy of the excitation forces. The propeller and main engine excitation forces were loaded separately on the finite element model to calculate the vibration velocity of each cabin, and the contribution of the two excitation sources to the vibration velocity of each cabin was analyzed. It was found that the contribution of the excitation source to the cabin response was related to the relative position between the cabin and the excitation source. When the cabin was located in the cabin adjacent to or directly above a certain excitation source, the contribution of the excitation source to the cabin response was greater. When the cabin was farther away from both excitation sources, the contribution of the propeller excitation was greater. This provides a targeted reference for the preliminary vibration assessment and later vibration control of the new polar expedition cruise ship.

Keywords: new polar exploration cruise; wet modal; admittance matrix; excited force; vibration contribute ratio



Citation: Jiang, G.; Yuan, Y.; Guo, H.; Wu, G.; Liu, Z. Vibration Characteristic Research of 100 m New Polar Exploration Cruise Based on Finite Element Modeling. *J. Mar. Sci. Eng.* **2024**, *12*, 779. <https://doi.org/10.3390/jmse12050779>

Academic Editor: Joško Parunov

Received: 11 April 2024

Revised: 1 May 2024

Accepted: 1 May 2024

Published: 7 May 2024



Copyright: © 2024 by the authors. Licensee MDPI, Basel, Switzerland. This article is an open access article distributed under the terms and conditions of the Creative Commons Attribution (CC BY) license (<https://creativecommons.org/licenses/by/4.0/>).

1. Introduction

As the primary mode of transportation at sea, the comfort and quietness of ships are increasingly emphasized. Reducing ship vibration and noise has gradually become the main breakthrough direction for ship designers [1,2]. The new 100 m polar expedition cruise ship is the first X-Bow polar expedition cruise ship made in China. The ship is characterized by a variety of systems, high power, and a complex hull structure with a meticulously designed engine room layout. The operation of the main power equipment makes the cabin of the ship prone to vibration and noise problems, which affect the comfort of the crew and passengers on board. In order to effectively control structural vibration and cabin noise in cruise ships, it is necessary to obtain input excitation from the main excitation source and to simulate and analyze their vibration characteristics during the design phase.

Wang et al. [3] deduced the propeller blade frequency excitation force under the conditions of known ship mass, stiffness, damping, and measured tail vibration velocity and

verified its accuracy, providing an effective method to determine the propeller excitation force. Pang et al. [4] studied the vibration characteristics of cylindrical shells by a semi-analytical method, solved the equations for the forced vibration characteristics of cylindrical shells, and analyzed the influence of boundary characteristics and structural parameters on the forced vibration of the cylindrical shells. Wang et al. [5,6] explored the vibration features of both a broad flat vessel and a river–sea-going container ship under various stimuli through experimentation and numerical computations. Gong and Zhang et al. [7] employed a local cabin finite element method (FEM) model and a single-cabin FEM model for a precise analysis of the grillage structure mode. He et al. [8] integrated the power flow theory of two-dimensional plates with the FEM, investigating the vibration transmission features of interconnected plates subjected to medium- to low-frequency excitation. Lu et al. [9] employed frequency spectrum analysis techniques to examine the vibration attributes of ship grillages and enhance the dynamic characteristics of such structures. Gao et al. [10] utilized the direct testing approach to examine the underwater vibration attributes of a standard stiffened cylindrical shell. The findings indicated that mechanical forces primarily affect high-frequency vibrations. Cao et al. [11] proposed a coupled vibration and noise source separation method based on operational transfer path analysis, treating multi-source signals as convolved, and established an OPA (operational transfer path analysis) model of a ship and verified the feasibility and correctness of the model by combining it with the ship transfer path vibration and sound test. Cheng et al. [12] simulated the vibration response of a super-large high-speed ship in the face of waves, studied the distribution of the vibration response along the length of the ship, and analyzed the variation in the vibration response with the sea state and speed and finally simulated and predicted the synthetic bending moment amidships and the whip effect based on three-dimensional time-domain nonlinear hydroelasticity theory. Based on the traditional transfer path principle, Lu et al. [13] propose an improved transfer path analysis technique based on weighted regularization and accurately identify the multi-source engine excitation loads, providing reliable vibration contribution analysis results. Zhang et al. [14] investigate the effects of structural design on vibration modes and transmission in ship multicabin structures, offering insights to enhance vibration protection in naval architecture.

In terms of foreign research, Jadee et al. [15] investigated the free vibration attributes of isotropic plates utilizing the FEM and experimental techniques. McVicar et al. [16] investigated the impact of slam force duration on the vibration response of a high-speed catamaran. Ogawa et al. [17], showing that hull girder vibration and ship operations substantially influence wave load statistics, caution against omitting them, as this could lead to overestimation errors. Prabhu et al. [18] conducted research on the structural dynamics and vibration characteristics of Marine Cycloidal Propeller (MCP) blades under maneuvering conditions, emphasizing the importance of analyzing fatigue and load variations in the design of the blades. Patil et al. [19] conducted an experimental and simulation-based analysis to optimize sound absorption materials in a 3.5-ton truck cabin, focusing on cost-effectiveness and rider comfort. Josip et al. [20] compared analytical and numerical methods for calculating hydrodynamic mass in ship vibration, finding good agreement but also suggesting the need for more research due to moderate differences between the approaches. These studies have provided us with a deeper understanding of the vibration characteristics of ships and laid the groundwork for further research.

To date, no vibration research has been conducted on this ship type in China. In this paper, a wet modal analysis, analysis of the main excitation sources, and calculation of the excitation sources' contributions to each compartment room for the prototype vessel are presented to provide design references for similar vessels to be constructed later. Figure 1 below shows a flowchart of the process of the proposed methodology.

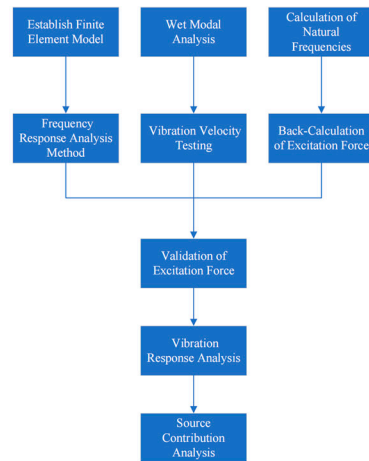


Figure 1. The flowchart of the process of the proposed method.

2. Method

2.1. Modal Analysis of New Polar Expedition Cruise Ship

To analyze the vibration characteristics of the polar expedition cruise ship, a finite element model was established. The model measures 104 m in length, 18 m in width, and has a waterline height of 5.1 m, with a mass of 4265 tons. The model's additional mass and center of gravity are strictly based on the weight and center of gravity report, as depicted in Figure 2. The primary grid size is 400×400 mm, with quad 4 and tria 3 elements utilized to model the slab structure using shell theory, bar2 elements for the beam structure, and a structural damping factor of 2% [21].

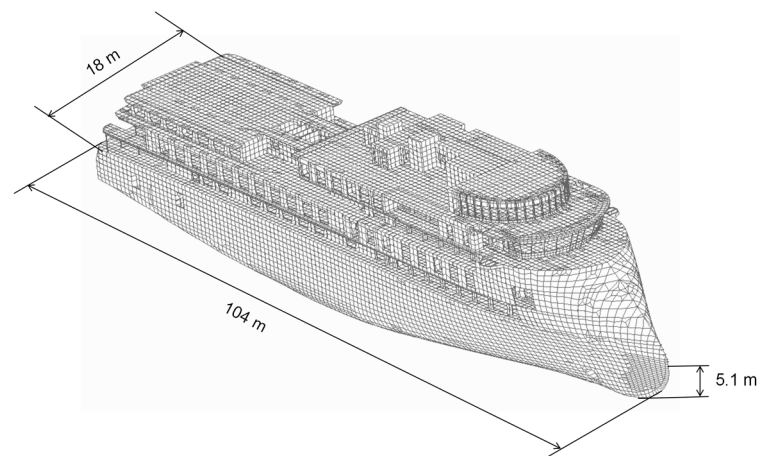


Figure 2. The finite element mesh model of the new polar expedition cruise ship.

The method of additional virtual mass is used for wet modal calculation, and the additional mass matrix is solved to reflect the effect of incompressible fluid on the structure, which is the core of the virtual mass method [22]. For undamped structures, the equation of the motion of the structure in the fluid–structure interaction is [23].

$$M_s \ddot{r} + K_s r - B^T p + f_0 = 0 \quad (1)$$

where M_s , K_s are the mass matrix and stiffness matrix of the structure, respectively, B is the fluid–structure interaction matrix, P is the fluid dynamic pressure, f_0 is the external excitation, r is the displacement vector of the structure, and \ddot{r} is the structural acceleration vector. The discretized fluid equations of motion can be expressed as follows:

$$H p + \rho B \ddot{r} + q_0 = 0 \quad (2)$$

where H is the fluid stiffness matrix, and ρ is the fluid density. Combining Equations (1) and (2), and when considering free vibration, we have

$$\begin{bmatrix} M_s & 0 \\ \rho B & 0 \end{bmatrix} \begin{bmatrix} \ddot{r} \\ \ddot{p} \end{bmatrix} + \begin{bmatrix} K_s & -B^T \\ 0 & H \end{bmatrix} \begin{bmatrix} r \\ p \end{bmatrix} = \begin{bmatrix} 0 \\ 0 \end{bmatrix} \quad (3)$$

Solving the above formula can obtain the following:

$$(M_s + M_a)\ddot{r} + K_s r = 0 \quad (4)$$

where $M_a = \rho B^T H^{-1} B$ is the added mass of the fluid (M_a and M_s are matrices).

Use the MFLUID card in Nastran to set the additional mass of the fluid. The setting procedure is as follows:

CEND

MFLUID = 1

.....

param, vmopt,1

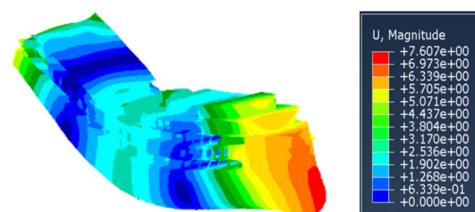
MFLUID, 1,5100.0,1.0-9, 1, N, N (Correct, the input rule in Nastran, means 1e-9)

ELIST,1,1, THRU,12227

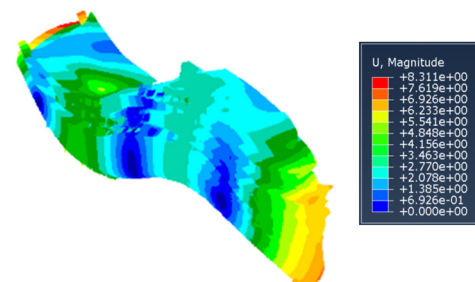
Using the virtual mass method for wet modal analysis, the first four natural frequencies and modal shapes of the new polar expedition cruise ship were obtained. Table 1 presents the natural frequencies for each mode, while Figure 3 illustrates the modal shapes. The possibility of structural resonance during operation can be assessed by comparing the structure's natural frequencies with the excitation frequencies resulting from mechanical components, including but not limited to the engine and propeller.

Table 1. The former fourth-order mode.

Mode Shape	Frequency (Hz)
vertical first order	2.7
vertical second order	5.4
twist first order	5.6
horizontal first order	6.4



(a)



(b)

Figure 3. Cont.

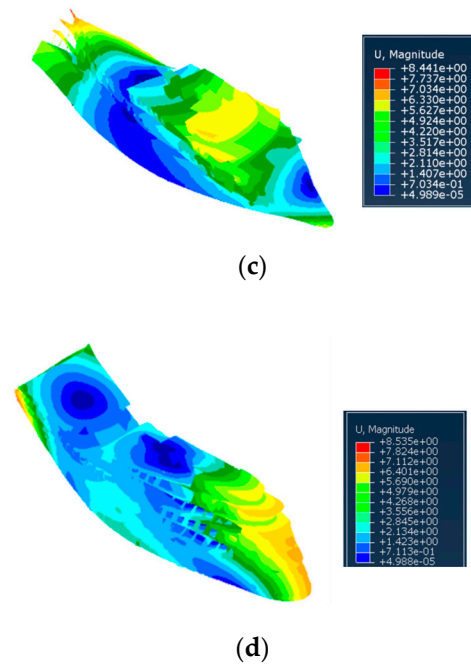


Figure 3. The shapes of the former fourth-order mode: (a) first-order vertical bending; (b) second-order vertical bending; (c) first-order twist; and (d) first-order lateral bending.

Frequency Comparison

The main reasons for the steady-state forced vibration of the ship are the unbalanced inertial force of the reciprocating machinery on board, the interference force caused by the propeller, and the cavitation near the high-speed vessel [24]. When the cruise ship sails at high speed, a large number of air bubbles are generated on the propeller blades, which results in the generation of extremely severe pulsating pressures on the ship's hull by the propeller blades [25]. According to research, the surface force induced by the spiral motion is the most important factor in the propeller vibration source [26]. Meanwhile, because the power equipment such as the gyro stabilizer is relatively small in power and vibration isolation devices are installed, their contribution to the vibration of each room compartment is minor. Therefore, the excitation sources considered in this paper only include the main engine excitation force and the propeller pulsation force.

The new polar expedition cruise ship adopts two propellers and two rudders, the propeller diameter is 3100 mm, and 80% of the rated working speed is 192 RPM; the propeller excitation blade frequency can be calculated by Equation (5):

$$f = \frac{n \times Z}{60} \quad (5)$$

where n is the rotational speed, and Z is the number of propeller blades, so the propeller pulsation excitation blade frequency can be obtained as 12.8 Hz.

The host firing frequency can be obtained from Equation (6):

$$f = \frac{nZ}{60} m \quad (6)$$

where n is the rotational speed, Z is the number of cylinders, and m is 0.5 for a four-stroke diesel engine.

The new polar expedition cruise ship has two kinds of four-stroke main engines where the main engine is 8-cylinder and 6-cylinder, respectively, and 80% of the rated working speed is 1000 RPM. By Equation (6), it can be known that the two main engine firing frequencies are 66.8 Hz and 50 Hz, respectively.

The machine fundamental frequency can be obtained from Equation (7):

$$f = \frac{n}{60} \quad (7)$$

It can be obtained that the fundamental frequency of both hosts is 16.7 Hz.

As can be seen from Table 1, the excitation main frequency is not in the range of the whole-ship resonance frequency under the 80% rated working condition, i.e., the new polar expedition cruise ship does not have the risk of resonance of the whole ship, which preliminarily verifies the rationality of the vibration characteristics of this ship type structure.

2.2. An Analysis of the Excitation Force of the New Polar Expedition Cruise Ship

Solving for the excitation force mainly uses the traditional transfer path analysis principle, which is applicable to linear, time-invariant systems [27], and the main principles are shown in Figure 4.

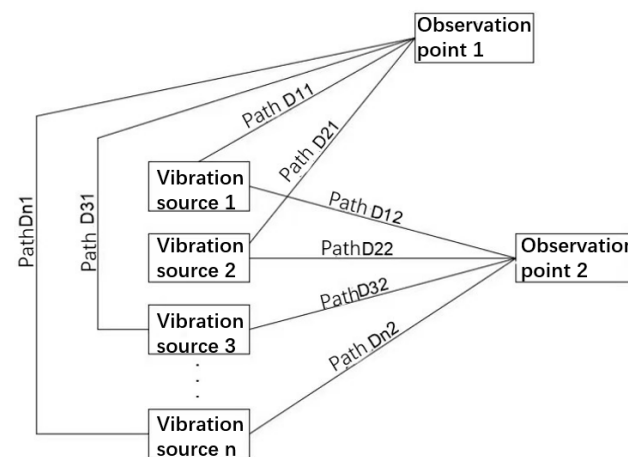


Figure 4. The sketch figure of the transmission path analysis.

Assuming that F_n is the excitation force of each source, v_m is the vibration velocity response of the observation point, and D_{nm} is the admittance of the transfer path from the excitation point n of the vibration source to the observation point m , Equation (8) can be obtained:

$$\begin{Bmatrix} V_1 \\ V_2 \\ \vdots \\ V_m \end{Bmatrix} = \begin{bmatrix} D_{11} & D_{21} & \cdots & D_{n1} \\ D_{12} & D_{22} & \cdots & D_{n2} \\ \vdots & \vdots & \ddots & \vdots \\ D_{1m} & D_{2m} & \cdots & D_{nm} \end{bmatrix} \begin{Bmatrix} F_1 \\ F_2 \\ \vdots \\ F_m \end{Bmatrix} \quad (8)$$

If v_m and D_{nm} are known, the above equation is multiplied left and right by the inverse matrix of the admittance matrix simultaneously to obtain Equation (9):

$$\begin{bmatrix} D_{11} & D_{21} & \cdots & D_{n1} \\ D_{12} & D_{22} & \cdots & D_{n2} \\ \vdots & \vdots & \ddots & \vdots \\ D_{1m} & D_{2m} & \cdots & D_{nm} \end{bmatrix}^{-1} \begin{Bmatrix} V_1 \\ V_2 \\ \vdots \\ V_m \end{Bmatrix} = \begin{Bmatrix} F_1 \\ F_2 \\ \vdots \\ F_n \end{Bmatrix} \quad (9)$$

In order to ensure that the equation has a solution, let $m = n$, and make the admittance matrix an $n \times n$ order matrix; the excitation force can be obtained.

2.2.1. Propeller Pulsation Excitation

The pulsating force on the bottom surface of the ship is the surface force of the propeller directly exciting the hull. In order to calculate the propeller pulsating excitation,

the vibration speed and transfer path admittance should be obtained. During the trial voyage of the new polar expedition cruise ship, the stern bottom plate directly above the propeller was selected as the test object, and a total of six measuring points were arranged, as shown in Figure 5, and the field test is shown in Figure 6. The data acquisition instrument is the INV3018CT high-precision collector, and the sensor is the INV9821 accelerometer, as shown in Figure 7. And the specific parameters are shown in Table 2; in order to avoid overlapping, the sampling frequency should be no less than 2.56 times the maximum test frequency, which is 250 Hz, and the sampling frequency is 1024 Hz.

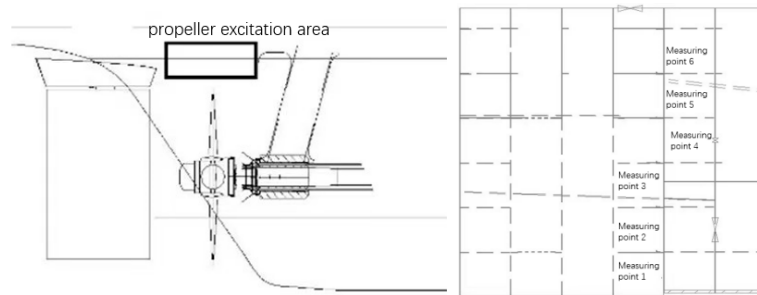


Figure 5. The arrangement of vibrated velocity test points.



Figure 6. The vibration test in site.

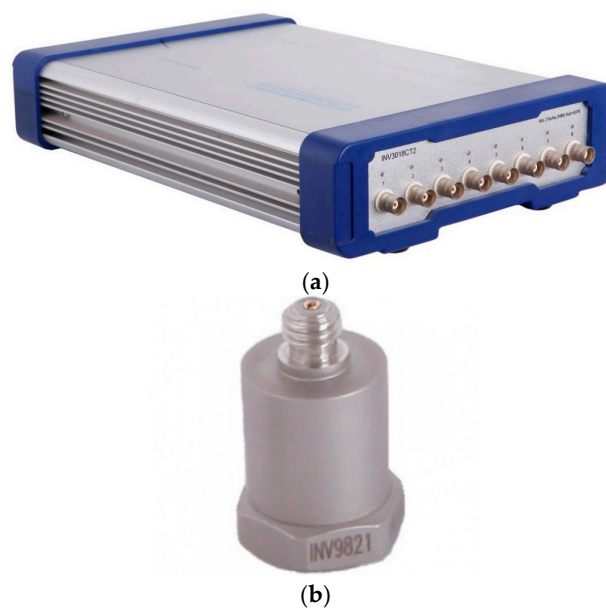
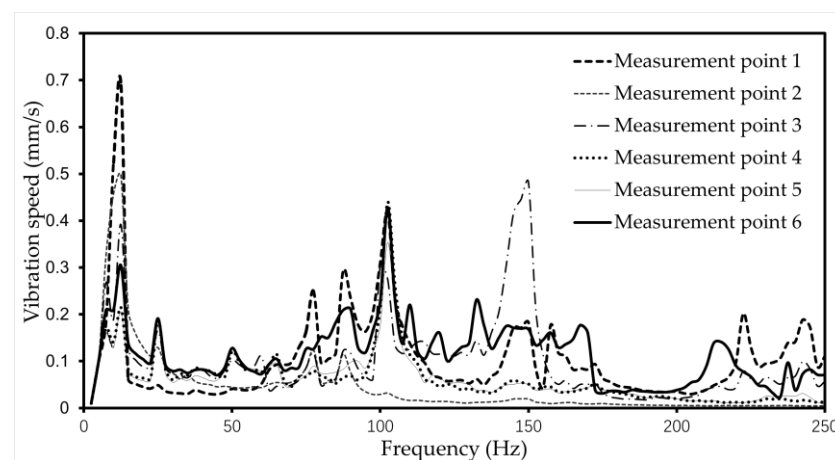


Figure 7. Data collectors and acceleration sensors. (a) INV3018CT high-precision collector; (b) INV9821 accelerometer.

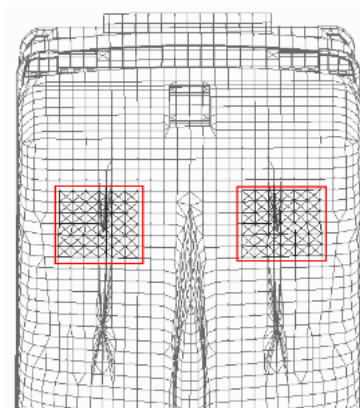
Table 2. Data collectors and accelerometer parameters.

Data Collectors		Acceleration Sensors	
Type	INV3018CT	Type	INV9821
Number of channels	8	Sensitivity	50 mV/g
AD accuracy	24 bits	Measuring range	100 g
Maximum sampling frequency	102.4 KHz	Resolution	0.001 m/s ²
Frequency of analysis	40 KHz	Operating voltage	18~28 VDC
Dynamic range	120 dB	Working power	2~20 mA
Application software	DASP	Output resistance	<100 Ω

The vibration velocity of the bottom plate of the ship directly above the propeller at 80% of the sailing conditions was obtained by testing, as shown in Figure 8; V_n represents the vibration speed of the measuring point n , $n = 1, 2, \dots, 6$.

**Figure 8.** The vibrated velocity of the hull plate above the propeller.

The propeller pulsation excitation is a non-uniformly distorted pressure field, so it is necessary to determine the propeller pulsation excitation area. A more practical method is to select the area above the propeller as about the square of the propeller diameter as the propeller pulsation excitation area [28], as shown in Figure 9.

**Figure 9.** The excited area of the propeller pulsatory force.

Since the propeller pulsation excitation is a non-uniformly distorted pressure field, a simplified method is needed to simulate the non-uniformly distorted pressure field. The port and starboard propeller pulsation excitation regions are divided into six force regions, which together carry the propeller non-uniformly distributed pressure field, while each

force region is a uniformly distributed pressure field. Denote by F_n the combined surface force carried by the n th force area, as shown in Figure 10.

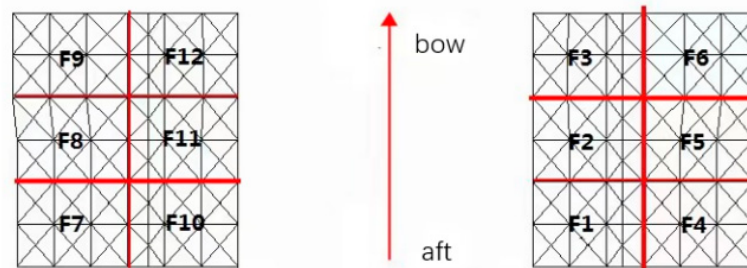


Figure 10. The partition of the excited area of the propeller pulsatory force.

In order to obtain the transfer path admittance from each force region to each observation region, let F_n be equal to 1 N ($n = 1, 2, 3, \dots, 12$) in the whole frequency band and load on each force region of the cruise ship finite element model, respectively, the frequency response analysis of each observation point to obtain the transfer path guide. Figure 10 shows the admittance curve from each propeller excitation force area to measurement point 1 on the starboard side. By comparing Figures 8 and 11, it can be found that the admittance curve is flat at 12.5 Hz and 25 Hz without resonant wave peaks, so the wave peak frequencies at 12.5 Hz and 25 Hz at the low frequency of the vibration velocity corresponds to the blade frequency and multi-blade frequency of the propeller pulsation excitation, while the admittance curve between 100 Hz and 150 Hz has an obvious resonance wave peak. Therefore, the wave peak frequency of the vibration velocity near 100 Hz and 150 Hz corresponds to the resonance frequency of the local structure of the ship bottom.

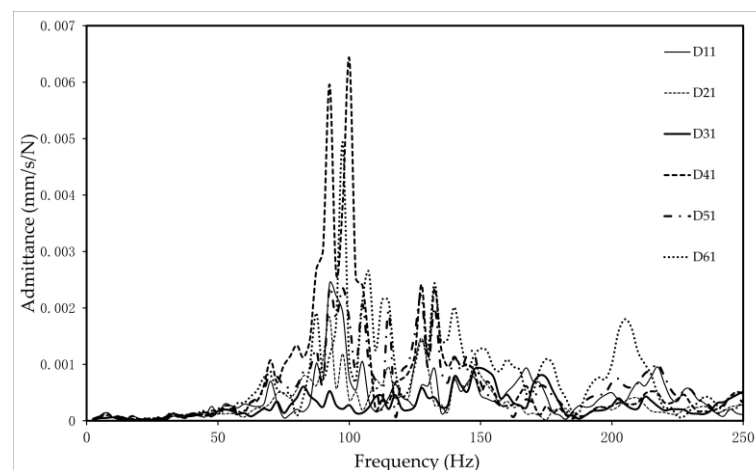


Figure 11. The admittances from the propeller excited area partitions to test point 1 in the starboard.

Due to the excitation of the host excitation force, it is necessary to consider whether the vibration velocity at the observation point of the host excitation force has an effect, so the nearest excitation point on the base of the host to the observation point is selected, and the unit force of the hull frequency band is loaded on the excitation point for a frequency response analysis and to obtain the transfer path admittance.

Figure 12 shows the comparison of the transfer path admittance from the host excitation point and the propeller excitation point 1 to the observation point 1; it can be seen from the figure that the admittance from the host excitation point to observation point 1 is much smaller than the admittance from the propeller excitation point to observation point 1, so the contribution of the host excitation to the velocity of the measurement point can be ignored when back-propelling the propeller pulsation excitation.

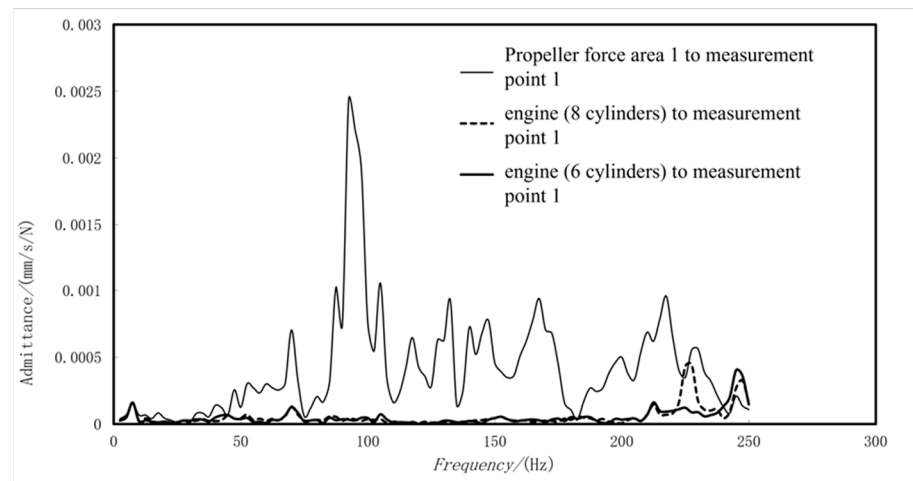


Figure 12. The comparison of admittances from excited sources to test point 1.

Substituting the transfer path admittance $D_{n,m}$ and the measurement point velocity V_n into Equation (7), we can obtain

$$\begin{Bmatrix} V_1 \\ V_2 \\ \vdots \\ V_6 \end{Bmatrix} = \begin{bmatrix} D_{1,1} & D_{2,1} & \cdots & D_{6,1} \\ D_{1,2} & D_{2,2} & \cdots & D_{6,2} \\ \vdots & \vdots & \ddots & \vdots \\ D_{1,6} & D_{2,6} & \cdots & D_{6,6} \end{bmatrix} \begin{Bmatrix} F_1 \\ F_2 \\ \vdots \\ F_6 \end{Bmatrix} + \begin{bmatrix} D_{7,1} & D_{8,1} & \cdots & D_{12,1} \\ D_{7,2} & D_{8,2} & \cdots & D_{12,2} \\ \vdots & \vdots & \ddots & \vdots \\ D_{7,6} & D_{8,6} & \cdots & D_{12,6} \end{bmatrix} \begin{Bmatrix} F_7 \\ F_8 \\ \vdots \\ F_{12} \end{Bmatrix} \quad (10)$$

Since the two propellers are arranged anti-symmetrically, the resultant surface forces should also be anti-symmetric, namely as follows:

$$\begin{cases} F_1 = F_7 & F_2 = F_8 & F_3 = F_9 \\ F_4 = F_{10} & F_5 = F_{11} & F_6 = F_{12} \end{cases} \quad (11)$$

So, Equation (10) can be transformed into the following:

$$\begin{Bmatrix} V_1 \\ V_2 \\ \vdots \\ V_6 \end{Bmatrix} = \begin{bmatrix} D_{1,1} + D_{7,1} & D_{2,1} + D_{8,1} & \cdots & D_{6,1} + D_{12,1} \\ D_{1,2} + D_{7,2} & D_{2,2} + D_{8,2} & \cdots & D_{6,2} + D_{12,2} \\ \vdots & \vdots & \ddots & \vdots \\ D_{1,6} + D_{7,6} & D_{2,6} + D_{8,6} & \cdots & D_{6,6} + D_{12,6} \end{bmatrix} \begin{Bmatrix} F_1 \\ F_2 \\ \vdots \\ F_6 \end{Bmatrix} \quad (12)$$

Multiplying the left and right side of Equation (12) by the inverse matrix of the admittance matrix at the same time, we can obtain

$$\begin{bmatrix} D_{1,1} + D_{7,1} & D_{2,1} + D_{8,1} & \cdots & D_{6,1} + D_{12,1} \\ D_{1,2} + D_{7,2} & D_{2,2} + D_{8,2} & \cdots & D_{6,2} + D_{12,2} \\ \vdots & \vdots & \ddots & \vdots \\ D_{1,6} + D_{7,6} & D_{2,6} + D_{8,6} & \cdots & D_{6,6} + D_{12,6} \end{bmatrix}^{-1} \begin{Bmatrix} V_1 \\ V_2 \\ \vdots \\ V_6 \end{Bmatrix} = \begin{Bmatrix} F_1 \\ F_2 \\ \vdots \\ F_6 \end{Bmatrix} \quad (13)$$

Based on the numerical solution of the above equation by MATLAB software (version R2020a), the final propeller pulsation excitation force can be obtained, as shown in Figure 13, which shows that the propeller pulsation excitation force is mainly distributed around the half-blade frequency 7 Hz, the blade frequency 12.5 Hz, and the multi-blade frequency 25 Hz, among which is the most obvious at the blade frequency.

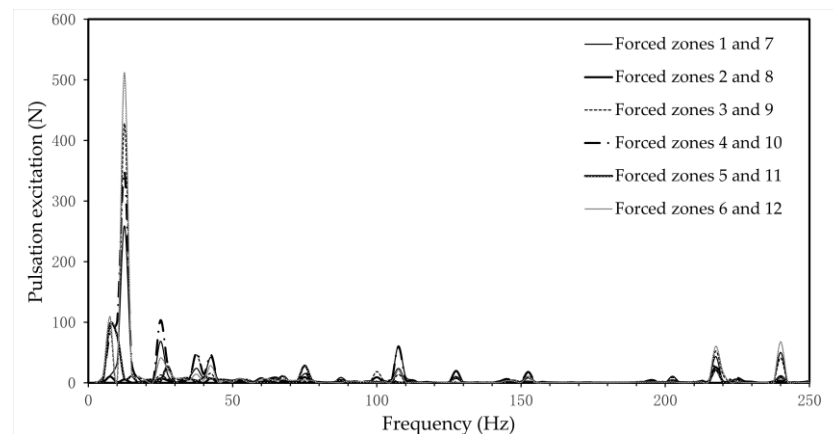


Figure 13. The propeller pulsatory excited force.

2.2.2. Host Incentive

The novel polar expedition cruise ship is equipped with four four-stroke main engines, featuring an integrated design where the main engine and generator systems are mechanically coupled, allowing for a shared power train and synchronized control systems. The layout of the main engine room is shown in Figure 14. Among them, main engine A and main engine C are Wartsila 8L20 with the maximum power of 1600 KW and the number of cylinders is 8, and the main engine B and main engine D model is Wartsila 6L20, the maximum power is 1200 KW, the number of cylinders is 6, and all rated speeds are 1000 RPM. From Equation (6), the firing frequency of host A and host C is 66.8 Hz, and the firing frequency of host B and host D is 50 Hz.

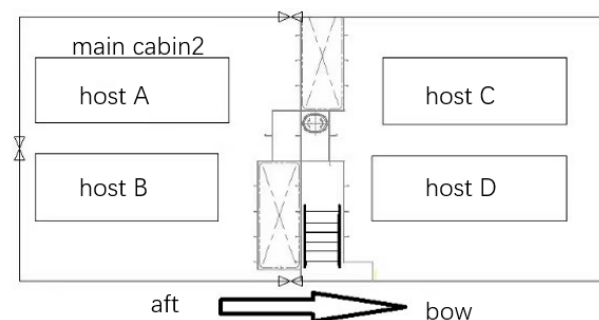


Figure 14. The layout of the main engines.

The measurement points are arranged and numbered at the bolted connection between the host engine and the base, and the finite element model of the host engine base and the numbering arrangement of the measuring points are shown in Figure 15. The vibration velocity was measured at measurement point 1, as shown in Figure 16. From Figure 16, it can be seen that the four main wave peak frequencies of the vibration velocity at main measuring point 1 are 12.5 Hz, 17.5 Hz, 25 Hz, 50 Hz, and 67.5 Hz, which correspond to the leaf frequency and the times leaf frequency of the propeller pulsation excitation and the fundamental frequency and firing frequency of the host engine, so it is necessary to consider the contribution of the propeller pulsation excitation to the vibration velocity of each measuring point and the interaction between the main engine when reversing the excitation force of the main engine.

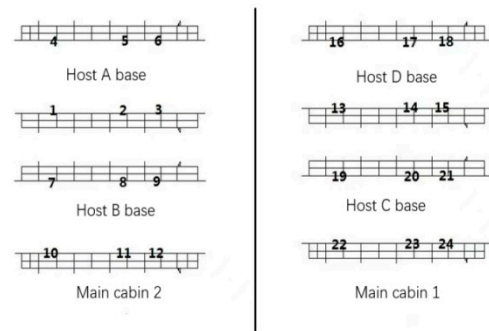


Figure 15. The finite model of the main engine foundations and the arrangement of test points.

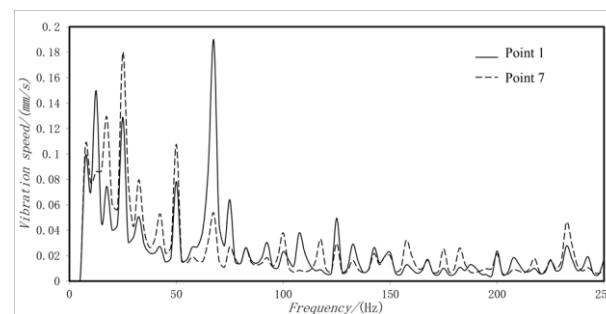


Figure 16. The vibrated velocity of test point 1 and 7.

In order to verify the interaction between the host excitation, the full-band unit force is applied at each foot on the host base, and a frequency response analysis is performed to obtain the admittance of each transfer path; using host A base measurement point 1 in main cabin 2 as the object of study, first analyze the influence of the adjacent cabin base, as shown in Figure 17, for the transfer path admittance from measurement points 1, 13, and 19 to measurement point 1. From Figure 17, it can be seen that the transfer path admittance between the two base measurement points 13 and 19 to measurement point 1 in main compartment 1 is much smaller than the measurement point 1 origin admittance, so the host excitation contribution in compartment 1 can be neglected when back-propagating the host excitation force in the host base of compartment 2.

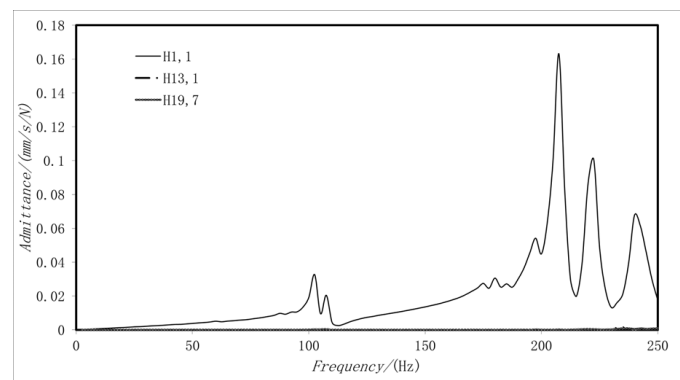


Figure 17. The admittances from test point 1, 13, and 19 to test point 1 (there are actually three curves in this figure, two of which have very small amplitudes and are attached to the x-axis.).

Taking measuring point 1 as the research object, the interaction of the excitation of each measurement point in main engine compartment 2 is analyzed, as shown in Figure 18, for the transfer path admittance from measurement points 1 to 3 and 4, 7 to 9, and 10 to measurement point 1.

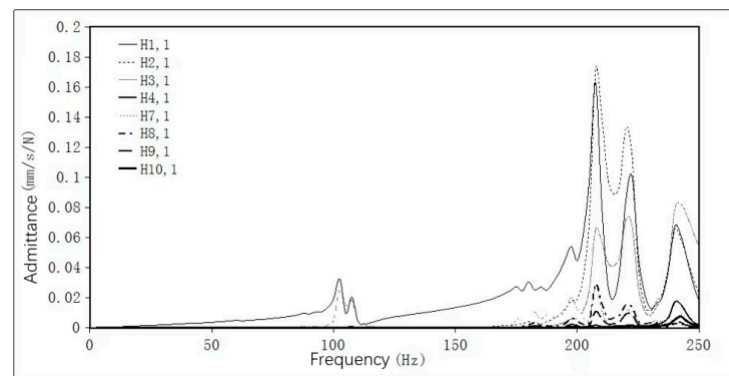


Figure 18. The admittances from test point 1~3 and 4, 7~9, and 10 to test point 1.

The transfer path admittance from measurement point 4 and measurement point 10 to measurement point 1 is also much smaller than the transfer path admittance from other measurement points to measurement point 1. Meanwhile, since measurement points 5, 6, 11, and 12 are farther away from measurement point 1, the excitation contribution of measurement points 4~6 and 10~12 to the measurement point can be ignored, and the same conclusion can be obtained by analyzing measurement points 2 and 3. Therefore, when back-projecting the excitation force of measurement points 1~3 and 7~9, the excitation contribution of points 4~6 and 10~12 can be ignored, but the self-excitation contribution of points 1~3 and 7~9 as well as the propeller pulsation excitation contribution should be considered, while when back-projecting the excitation force of points 4~6, only the propeller pulsation excitation contribution and the self-excitation contribution of points 4~6 need to be considered. Let U_n denote the vibration velocity at the base of the machine foot, T_n denote the vertical excitation at the machine foot, M_{mn} denote the transfer path admittance from the propeller pulsation excitation region to the main engine base, and H_{mn} denote the transfer path admittance between the main engine bases, so Equation (14) can be obtained:

$$\begin{aligned}
 \begin{Bmatrix} U_1 \\ U_2 \\ U_3 \\ U_7 \\ U_8 \\ U_9 \end{Bmatrix} &= \begin{bmatrix} M_{1,1} + M_{7,1} & M_{2,1} + M_{8,1} & \cdots & M_{6,1} + M_{12,1} \\ M_{1,2} + M_{7,2} & M_{2,2} + M_{8,2} & \cdots & M_{6,2} + M_{12,2} \\ M_{1,3} + M_{7,3} & M_{2,3} + M_{8,3} & \cdots & M_{12,3} + M_{12,3} \\ M_{1,7} + M_{7,7} & M_{2,7} + M_{8,7} & \cdots & M_{12,7} + M_{12,7} \\ M_{1,8} + M_{7,8} & M_{2,8} + M_{8,8} & \cdots & M_{12,8} + M_{12,8} \\ M_{1,9} + M_{7,9} & M_{2,9} + M_{8,9} & \cdots & M_{12,9} + M_{12,9} \end{bmatrix} \begin{Bmatrix} F_1 \\ F_2 \\ \vdots \\ F_6 \end{Bmatrix} \\
 &+ \begin{bmatrix} H_{1,1} & H_{2,1} & H_{3,1} & H_{7,1} & H_{8,1} & H_{9,1} \\ H_{1,2} & H_{2,2} & H_{3,2} & H_{7,2} & H_{8,2} & H_{9,2} \\ H_{1,3} & H_{2,3} & H_{3,3} & H_{7,3} & H_{8,3} & H_{9,3} \\ H_{1,7} & H_{2,7} & H_{3,7} & H_{7,7} & H_{8,7} & H_{9,7} \\ H_{1,8} & H_{2,8} & H_{3,8} & H_{7,8} & H_{8,8} & H_{9,8} \\ H_{1,9} & H_{2,9} & H_{3,9} & H_{7,9} & H_{8,9} & H_{9,9} \end{bmatrix} \begin{Bmatrix} T_1 \\ T_2 \\ T_3 \\ T_7 \\ T_8 \\ T_9 \end{Bmatrix} \quad (14)
 \end{aligned}$$

Through the above formula, it can be calculated that the excitation force at points 1, 2, 3, 7, 8, and 9 is as follows:

$$\begin{bmatrix} H_{1,1} & H_{2,1} & H_{3,1} & H_{7,1} & H_{8,1} & H_{9,1} \\ H_{1,2} & H_{2,2} & H_{3,2} & H_{7,2} & H_{8,2} & H_{9,2} \\ H_{1,3} & H_{2,3} & H_{3,3} & H_{7,3} & H_{8,3} & H_{9,3} \\ H_{1,7} & H_{2,7} & H_{3,7} & H_{7,7} & H_{8,7} & H_{9,7} \\ H_{1,8} & H_{2,8} & H_{3,8} & H_{7,8} & H_{8,8} & H_{9,8} \\ H_{1,9} & H_{2,9} & H_{3,9} & H_{7,9} & H_{8,9} & H_{9,9} \end{bmatrix}^{-1} \begin{pmatrix} U_1 \\ U_2 \\ U_3 \\ U_7 \\ U_8 \\ U_9 \end{pmatrix} - \begin{pmatrix} M_{1,1} + M_{7,1} & M_{2,1} + M_{8,1} & \cdots & M_{6,1} + M_{12,1} \\ M_{1,2} + M_{7,2} & M_{2,2} + M_{8,2} & \cdots & M_{6,2} + M_{12,2} \\ M_{1,3} + M_{7,3} & M_{2,3} + M_{8,3} & \cdots & M_{6,3} + M_{12,3} \\ M_{1,7} + M_{7,7} & M_{2,7} + M_{8,7} & \cdots & M_{6,7} + M_{12,7} \\ M_{1,8} + M_{7,8} & M_{2,8} + M_{8,8} & \cdots & M_{6,8} + M_{12,8} \\ M_{1,9} + M_{7,9} & M_{2,9} + M_{8,9} & \cdots & M_{6,9} + M_{12,9} \end{pmatrix} \begin{pmatrix} F_1 \\ F_2 \\ \vdots \\ F_6 \end{pmatrix} = \begin{pmatrix} T_1 \\ T_2 \\ T_3 \\ T_7 \\ T_8 \\ T_9 \end{pmatrix} \quad (15)$$

The excitation forces at points 4, 5, and 6 and 10, 11, and 12 are, respectively:

$$\begin{bmatrix} H_{4,4} & H_{5,4} & H_{6,4} \\ H_{4,5} & H_{5,5} & H_{6,5} \\ H_{4,6} & H_{5,6} & H_{6,6} \end{bmatrix}^{-1} \begin{pmatrix} U_4 \\ U_5 \\ U_6 \end{pmatrix} - \begin{pmatrix} D_{1,4} + D_{7,4} & D_{2,4} + D_{8,4} & \cdots & D_{6,4} + D_{12,4} \\ D_{1,5} + D_{7,5} & D_{2,5} + D_{8,5} & \cdots & D_{6,5} + D_{12,5} \\ D_{1,6} + D_{7,6} & D_{2,6} + D_{8,6} & \cdots & D_{6,6} + D_{12,6} \end{pmatrix} \begin{pmatrix} F_1 \\ F_2 \\ \vdots \\ F_6 \end{pmatrix} = \begin{pmatrix} T_4 \\ T_5 \\ T_6 \end{pmatrix} \quad (16)$$

$$\begin{bmatrix} H_{10,10} & H_{11,10} & H_{12,10} \\ H_{10,11} & H_{11,11} & H_{12,11} \\ H_{10,12} & H_{11,12} & H_{12,12} \end{bmatrix}^{-1} \begin{pmatrix} U_{10} \\ U_{11} \\ U_{12} \end{pmatrix} - \begin{pmatrix} D_{1,10} + D_{7,10} & D_{2,10} + D_{8,10} & \cdots & D_{6,10} + D_{12,10} \\ D_{1,11} + D_{7,11} & D_{2,11} + D_{8,11} & \cdots & D_{6,11} + D_{12,11} \\ D_{1,12} + D_{7,12} & D_{2,12} + D_{8,12} & \cdots & D_{6,12} + D_{12,12} \end{pmatrix} \begin{pmatrix} F_1 \\ F_2 \\ \vdots \\ F_6 \end{pmatrix} = \begin{pmatrix} T_{10} \\ T_{11} \\ T_{12} \end{pmatrix} \quad (17)$$

To simplify processing, let

$$T_{AC} = \frac{\sqrt{\sum (T_n)^2}}{6} \quad n = 1, 2, \dots, 6 \quad (18)$$

$$T_{BD} = \frac{\sqrt{\sum (T_m)^2}}{6} \quad m = 7, 8, \dots, 12 \quad (19)$$

where T_{AC} is the excitation force of hosts A and C, and T_{BD} is the excitation force of hosts B and D. After numerical calculation based on MATLAB software (version R2020a), the spectrum of T_{AC} and T_{BD} are obtained as shown in Figure 19.

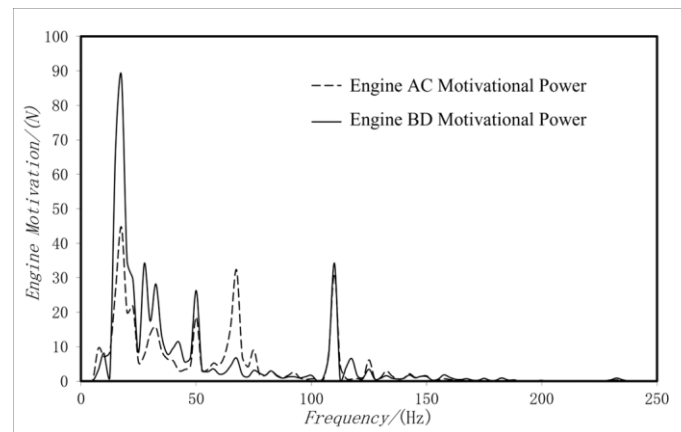


Figure 19. The main engines' excited force.

2.2.3. Excitation Force Validation

In order to verify the accuracy of the excitation force, the propeller pulsation excitation force and the main engine excitation were applied to the finite element model for spectrum analysis, and four areas close to the excitation source were selected: the second deck—laundry room, the second deck—crew room, the third deck—stern storage room, and the fourth deck—passenger cabin, and the simulation analysis results of these four areas are compared with the test results, and the comparison results are shown in Figures 20–23. It can be seen from the figure that the variation trend of the simulation curve and the test curve is consistent, and the effective value of the vibration speed is compared, as shown in Table 3, and the maximum error is 21%, which meets the engineering accuracy requirements. However, there are still some errors, which are mainly caused by two aspects: (1) the dressing, outfitting, interior, and other components are omitted in the finite element model, such as the four-layer deck—passenger cabin with floating bottom plates, interior partitions, and other components, which affect the transfer path admittance to a certain extent; and (2) in actual measurement, the cruise ship is also affected by wind and waves, pumps, steering gear, fans, and other excitation, such as the third deck—transom storage room, which is affected by the air compressor in the neighboring cabin, so the error is relatively large compared to other areas.

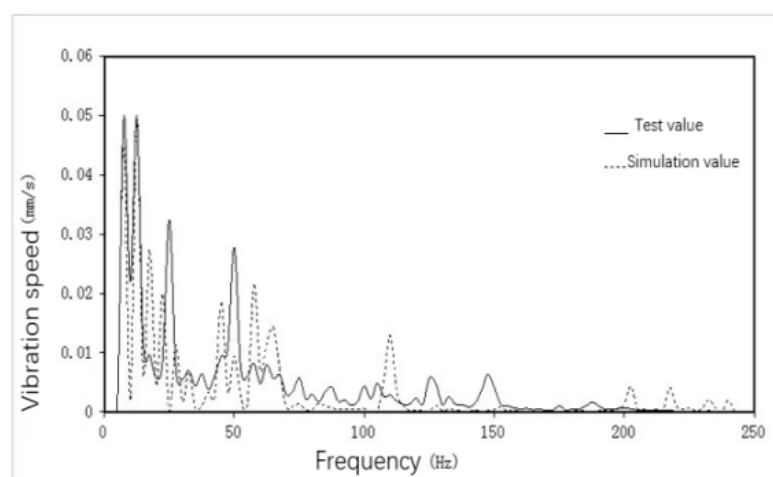


Figure 20. The laundry room on deck 2.

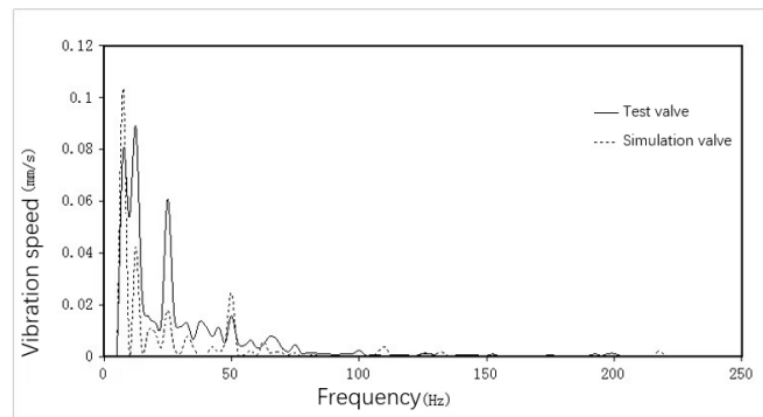


Figure 21. The crew room on deck 3.

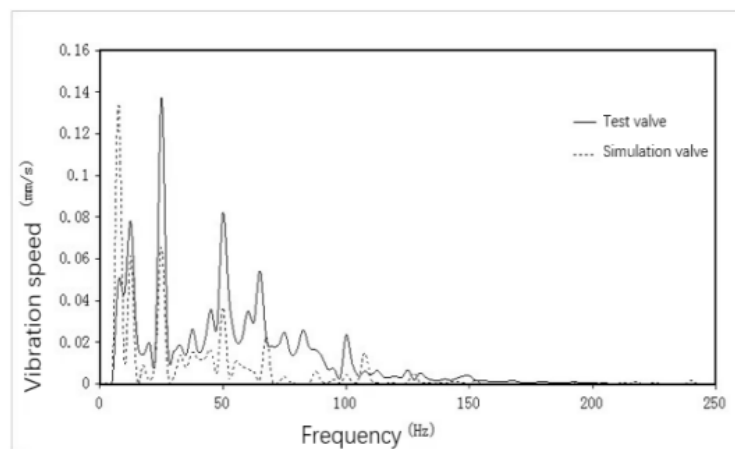


Figure 22. The outdoor area in the stern on deck 3.

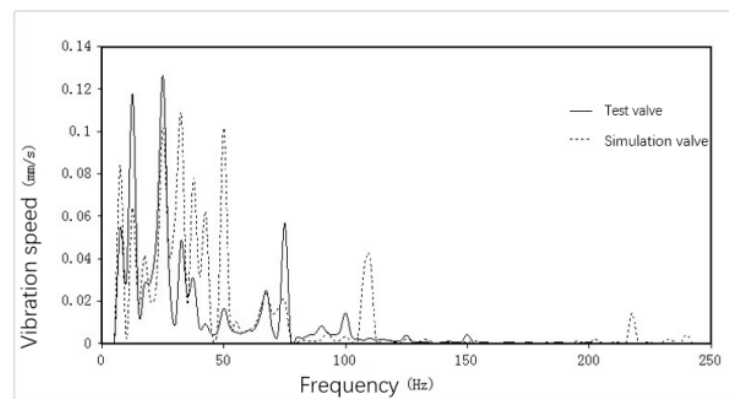


Figure 23. The passenger room on deck 4.

Table 3. The comparison between the affective value of the vibration velocity of the simulation and test.

	Test Valve (mm/s)	Simulation Value (mm/s)	Error
Second Deck—Laundry Center	0.09	0.08	6%
Second Deck—Crew Room Center	0.15	0.13	13%
Three Decks—Aft Storage Center	0.23	0.18	21%
Fourth Deck—Passenger Cabin Center	0.22	0.26	18%

3. Vibration Source Contribution Rate Analysis

In the contribution analysis, the following formula is generally used to calculate the vibration contribution of the path corresponding to each load at the target point [5].

$$C_{n,m}^{contri} = H_{n,m}^X F_m \quad (20)$$

That is, this is the response to the system generated by each excitation source separately. The propeller pulsation excitation and the main engine excitation were separately loaded on the finite element model of the new polar expedition cruise ship, and the frequency response analysis was performed. Typical compartments were selected, and the response contributions of the propeller pulsation excitation and main engine excitation to these compartments were compared, as shown in Table 4. It can be seen from the table, among the compartment on the second and third decks, except for the laundry room which is located directly above the main engine cabin, that the contribution of the main engine excitation is relatively large, and the contribution of the propeller excitation in the other cabins is relatively large. The two cabins on the fourth deck are located at the stern, so the contribution of the propeller excitation is relatively large. The two cabins on the fifth deck are located directly above the main engine cabin and are far from the stern, so the main engine excitation contribution is larger; among the compartments on the sixth and seventh decks, the gym is located in the position directly above the main engine cabin, and the contribution of the main engine excitation is relatively large, while the other three compartments are farther away from both excitation sources, and the contribution of the propeller excitation is relatively large. Through the above analysis, it can be seen that for the new polar expedition cruise ship, the contribution of the excitation source to the cabin response is related to the relative position between the cabin and the excitation source; when the cabin is located in a cabin adjacent to or directly above the excitation source, the contribution of the excitation source to the cabin response is larger; when the cabin is far from both excitation sources, the contribution of the propeller excitation is larger, which is due to the smaller loss of the low frequency bending wave generated by the propeller excitation, which is easier to propagate.

Table 4. The comparison of the excited sources' contribution to the affective value of the classic cabin response.

Deck Level	Area	Response from Propeller Excitation (mm/s)	Propeller Incentive Contribution	Host Stimulus Response (mm/s)	Host Incentive Contribution
second deck	laundry room	0.038	47.5%	0.042	52.5%
	crew room	0.1	76.9%	0.03	23.1%
three decks	Stern storage room	0.15	83.3%	0.03	16.7%
	passenger compartment	0.08	80.0%	0.02	20.0%
four decks	Aft open area	0.24	58.5%	0.17	41.5%
	passenger compartment	0.14	53.8%	0.12	46.2%
five decks	Dining room	0.12	30.0%	0.28	70.0%
	kitchen	0.3	46.2%	0.35	53.8%
six decks	passenger compartment	0.035	57.4%	0.026	42.6%
	aisle	0.09	69.2%	0.04	30.8%
seven decks	Gym	0.04	18.2%	0.18	81.8%
	cab	0.08	88.9%	0.01	11.1%

4. Conclusions

The 100 m new polar expedition cruise ship is the first X-BOW polar expedition cruise ship made in China. There is no vibration research on this ship type in China for the time being, and this paper conducts a study on the vibration characteristics and excitation force contribution of the parent ship to provide a design reference for later-made ships of the same type.

1. The whole-ship resonance risk of the new polar expedition cruise ship is assessed. In this paper, a finite element model of the new 100 m polar expedition cruise ship is developed, and the additional mass and center of gravity of the model are adjusted in strict accordance with the weight and center of gravity report and interior weight data of the parent ship. Based on the virtual mass method, the wet modes of the entire ship of the new polar expedition cruise ship are analyzed. The first four main modes are 2.7 Hz, 5.4 Hz, 5.6 Hz, and 6.4 Hz, respectively, while the main excitation frequency of the propeller is 12.8 Hz, and the fundamental frequency of the main engine is 16.7 Hz. The firing frequencies are 50 Hz and 66.8 Hz, respectively, which are different from the first four main modal frequencies of the new polar expedition cruise ship. Based on the modal analysis, there is no significant risk of resonance for the ship, as the calculated natural frequencies do not coincide with the primary excitation frequencies of the ship's propulsion systems. In addition, this study utilizes finite element modeling and the virtual mass method to analyze the wet modal characteristics of a novel polar expedition cruise ship. Meanwhile, reference [14] explores the effects of structural factors on the vibrational characteristics of ships. Together, they highlight the integrated application value of diverse analytical techniques in the field of ship design.
2. It is difficult to obtain the excitation force of the ship, especially the spiral pulsation excitation, as the calculation theory is complicated, the experiment cost is high, and it is very unfriendly to shipyard workers. In this paper, based on the principle of transfer path analysis, the vibration velocity at the bottom plate above the propeller and the base of the main engine's foundation is tested. The finite element model of the new polar expedition cruise ship is used to calculate the transfer path admittance from the excitation point to the vibration velocity measurement point, and the coherence between each excitation source is analyzed to invert the propeller pulsation excitation and the main engine excitation. The two excitation sources are loaded in the finite element model for frequency response analysis, and the vibration response of each compartment is obtained. Four compartments nearer to the excitation source are selected, and the simulation values of the vibration response of these four compartments are compared with the test values. The trends of the frequency response curves are essentially consistent, and the error of the effective value of the vibration response is within 21%, which meets the requirements of the project progress and verifies the accuracy of the propeller pulsation excitation and the main engine excitation. Concurrently, the identified excitation forces can be instrumental in the vibration analysis of similar ship types, offering a valuable reference for the detailed design phase of such vessels. While the precision of the excitation forces has been corroborated through empirical testing, discrepancies observed in this study could be attributable to the simplifications inherent in the model or the complexities inherent to real-world maritime environments.
3. In the vibration control stage, it is necessary to adopt the targeted control of each type of excitation source separately. Therefore, it is necessary to obtain the contribution of each excitation source to the cabin room in order to propose a targeted control plan. The two excitation forces are separately loaded on the finite element model, and a frequency response analysis is carried out. A total of 12 typical cabins are selected, and the contribution of these two excitations to the responses of each cabin is analyzed. It is found that the percentage of the contribution of the excitation source to the response of the compartment is related to the relative position between the cabin

and the excitation source. When the cabin is located in the adjacent cabin or directly above the position of an excitation source, the contribution of this excitation source to the cabin response is larger. When the cabin is far away from both excitation sources, the contribution of the propeller excitation is larger, providing a reference for the later vibration control of the same type of ship.

Author Contributions: Conceptualization, G.J. and Y.Y.; methodology, G.J.; software, Z.L.; validation, G.J., Y.Y. and G.W.; formal analysis, H.G.; investigation, G.J.; resources, G.J.; data curation, Z.L. writing—original draft preparation, G.J.; writing—review and editing, Y.Y.; visualization, G.J.; supervision, G.J.; project administration, G.J.; funding acquisition, G.J. All authors have read and agreed to the published version of the manuscript.

Funding: Supported by the Science and Technology Commission of Shanghai Municipality and Shanghai Engineering Research Center of Ship Intelligent Maintenance and Energy Efficiency (Grant No. 20DZ2252300).

Data Availability Statement: Data is contained within the article.

Conflicts of Interest: The author declares that there are no conflicts of interest regarding the publication of this paper.

References

- Cheng, L.; He, J.L. Anti-vibration design method for 300000 DWT FPSO engine room. *Chin. J. Ship Res.* **2020**, *15*, 68–73.
- Choi, W.S.; Hong, S.Y.; Kwon, H.W.; Seo, J.H.; Rhee, S.H.; Song, J.H. Estimation of turbulent boundary layer induced noise using energy flow analysis for ship hull designs. *Proceedings of the Institution of Mechanical Engineers Part M. J. Eng. Marit. Environ.* **2020**, *234*, 196–208.
- Wang, M.; Zhao, D. New prediction method for the vibration response of hull girder by propeller excitation. *J. Ship Mech.* **2006**, *10*, 18–24.
- Pang, F.; Peng, D.; Li, H.; Tian, H.; Shan, Y. Forced vibration characteristics analysis of a cylindrical shell structure. *J. Vib. Shock* **2019**, *38*, 7–13.
- Wang, Y.W.; Wu, W.G.; Soares, C.G. Experimental and numerical study of the hydroelastic response of a river-sea going container ship. *J. Mar. Sci. Eng.* **2020**, *8*, 978. [\[CrossRef\]](#)
- Wang, Y.W.; Wu, W.G.; Zheng, C. The springing investigation of the wide flat ship type. *J. Vib. Shock* **2020**, *39*, 174–180.
- Gong, H.; Zhang, S.L. Study on the simplified modeling methods of ship grillage for modal analysis. *Ship Ocean Eng.* **2016**, *45*, 47–49, 54.
- He, P.; Xiang, Y.; Zhou, Y.; Li, H.R. Vibration energy distribution and transfer characteristics of coupled plates under medium-low frequency excitation. *Noise Vib. Control* **2020**, *4002*, 13–22.
- Lu, Z.Z. Dynamic optimization design of the plate frame structure of large ships. *Ship Sci. Technol.* **2021**, *4302*, 4–6.
- Gao, C.; Zhang, H.; Li, H.C.; Pang, F.Z.; Wang, H.F. Numerical and experimental investigation of vibro-acoustic characteristics of a submerged stiffened cylindrical shell excited by a mechanical force. *Ocean Eng.* **2022**, *249*, 110913. [\[CrossRef\]](#)
- Cao, Y.; Zhang, L.; Yang, Z. A new OPA model for ship noise sources and test validation. *J. Vib. Shock* **2013**, *32*, 158–162.
- Chen, Z.; Ren, H.; Li, H. Application of hydroelasticity theory and segmented model test in hull vibration response analysis. *J. Vib. Shock* **2012**, *31*, 119–124.
- Lu, G.; Luo, Y.; Zhang, X.; Xie, S.; Li, L.; Ma, C. Vibration transfer path analysis of rocket engine based on weighted regularization. *J. Vib. Shock* **2019**, *38*, 271–276.
- Zhang, C.; Yi, X.; Ma, W.; Wang, Y.; Li, H. Study on the influence of structural form and parameters on vibration characteristics of typical ship structures. *Rev. Adv. Mater. Sci.* **2022**, *61*, 16–26. [\[CrossRef\]](#)
- Jadee, K.J.; Abed, B.H.; Battawi, A.A. Free vibration of isotropic plates with various cutout configurations using finite elements and design of experiments. *IOP Conf. Ser. Mater. Sci. Eng.* **2020**, *745*, 012080. [\[CrossRef\]](#)
- McVicar, J.; Thomas, G.; Lavroff, J.; Davis, M.R. Effect of slam force duration on the vibratory response of a lightweight high-speed wave-piercing catamaran. *J. Ship Res.* **2015**, *59*, 69–84. [\[CrossRef\]](#)
- Ogawa, Y.; Takagi, K. An assessment of the effect of hull girder vibration on the statistical characteristics of wave loads. *Int. J. Nav. Archit. Ocean Eng.* **2011**, *3*, 80–85. [\[CrossRef\]](#)
- Prabhu, J.; Nagarajan, V.; Dash, A.K. Stochastic finite element analysis of composite cycloidal propeller blade during crash-stop ship maneuver. *Compos. Struct.* **2022**, *286*, 115306.
- Patil, S.; Bano, F.; Kurahatti, R.V.; Patil, A.Y.; Raju, G.U.; Afzal, A.; Soudagar, M.E.M.; Kumar, R.; Saleel, C.A. A study of sound pressure level (SPL) inside the truck cabin for new acoustic materials: An experimental and FEA approach. *Alex. Eng. J.* **2021**, *60*, 5949–5976. [\[CrossRef\]](#)
- Bašić, J.; Parunov, J. Analytical and Numerical Computation of Added Mass in Ship Vibration Analysis. *Brodogr. Asopis Brodogr. I Brodogr. Ind.* **2013**, *64*.

21. DNVGL. *Vibration Analysis Report*; U11058_101-012, 2018; DNV: Bærum, Norway, 2018.
22. Gao, S.Y. Calculation and Characteristic Analysis of Vibration and Noise of Underwater Shell Structure Based on Virtual Mass Method. Master Dissertation, Harbin Engineering University, Harbin, China, 2015.
23. Liu, R.; Hao, Z.; Zheng, X. Transfer path analysis of ship structure-borne noises based on the Warshall-Floyd algorithm. *J. Vib. Shock* **2019**, *36*, 199–204.
24. Jin, X.; Xia, L. *Hull Vibration*; Shanghai Jiaotong University Press: Shanghai, China, 2011.
25. Hajime, T. Estimate of Surface Force Induced by Propeller. *Soc. Nav. Archit. Jpn.* **1976**, *140*, 49–67.
26. He, Y.; Wang, G. *Propeller Excitation Force*; Shanghai Jiaotong University Press: Shanghai, China, 1987.
27. Cinkraut, J. *Transfer Path Analysis of a Passenger*; Royal Institute of Technology: Stockholm, Sweden, 2016.
28. Veritas, D.N. *Prevention of Harmful Vibration in Ships*; DNV: Bærum, Norway, 1983.

Disclaimer/Publisher’s Note: The statements, opinions and data contained in all publications are solely those of the individual author(s) and contributor(s) and not of MDPI and/or the editor(s). MDPI and/or the editor(s) disclaim responsibility for any injury to people or property resulting from any ideas, methods, instructions or products referred to in the content.